Exploiting Fine-grained Dimming with Improved LiFi Throughput

XIAO ZHANG, Michigan State University, East Lansing, USA
JAMES MARIANI, Michigan State University, East Lansing, USA
LI XIAO, Michigan State University, East Lansing, USA
MATT W. MUTKA, Michigan State University, East Lansing, USA

Optical wireless communication (OWC) shows great potential due to its broad spectrum and the exceptional intensity switching speed of LEDs. Under poor conditions, most OWC systems switch from complex and more error prone high-order modulation schemes to more robust On-Off Keying (OOK) modulation defined in the IEEE OWC standard. This paper presents LiFOD, a high-speed indoor OOK-based OWC system with fine-grained dimming support. While ensuring fine-grained dimming, LiFOD remarkably achieves robust communication at up to 400 Kbps at a distance of 6 meters. This is the first time that the data rate has improved via OWC dimming in comparison to the previous approaches that consider trading off dimming and communication. LiFOD makes two key technical contributions. First, LiFOD utilizes Compensation Symbols (CS) as a reliable side-channel to represent bit patterns dynamically and improve throughput. We firstly design greedy-based bit pattern mining. Then we propose 2D feature enhancement via YOLO model for real-time bit pattern mining. Second, LiFOD synchronously redesigns optical symbols and CS relocation schemes for fine-grained dimming and robust decoding. Experiments on low-cost Beaglebone prototypes with commercial LED lamps and the photodiode (PD) demonstrate that LiFOD significantly outperforms the state-of-art system with 2.1x throughput on the SIGCOMM17 data-trace.

CCS Concepts: • **Networks** → *Mobile networks*; **Wireless personal area networks**; • **Human-centered computing** → *Mobile devices*; **Ubiquitous and mobile computing**.

Additional Key Words and Phrases: compensation symbol, side channel, LiFi, deep learning, and optical wireless communication.

1 INTRODUCTION

LiFi (Light Fidelity) is closely related to sensor networks since it uses visible light as medium for optical wireless communication to send data, giving sensor networks a dependable and fast wireless communication option by utilizing the LED bulbs already installed everywhere. This makes it easier for sensor data to be collected and transmitted quickly and effectively. Recent trends in indoor lighting include replacing incandescent and fluorescent bulbs with high-intensity LEDs because of their high energy efficiency, low heat generation, and long lifespan[1–4]. LED lighting saves the average family approximately $225 in electricity bills each year[5]. Another benefit of LEDs is their capability to switch between different light intensities quickly[6]. This feature creates opportunities for LEDs to be used as OWC transmitters for both high-speed communication and efficient lighting in everyday situations[7]. However, even with LED bulbs, lighting still accounts for around 15% of an ordinary home's electricity use[5]. Thus, for indoor LED bulbs, **transmitting more data robustly** with less

Authors' addresses: Xiao Zhang, zhan1387@msu.edu, Michigan State University, East Lansing, USA; James Mariani, mariani4@msu.edu, Michigan State University, East Lansing, USA; Li Xiao, lxiao@cse.msu.edu, Michigan State University, East Lansing, USA; Matt W. Mutka, mutka@msu.edu, Michigan State University, East Lansing, USA.

ACM 1550-4859/2024/2-ART
https://doi.org/10.1145/3643814

retransmission while **not sacrificing the user experience of lighting** is another path to improve energy efficiency.

Recent research has concentrated on enhancing throughput in Optical Wireless Communication (OWC) systems through the utilization of high-order modulation techniques[6, 8–10]. However, in poor optical channel conditions, such as indoor scenarios with complex artificial light sources or with sunny or underwater outdoor scenarios, the nonlinear effect of LEDs and the short symbol distance make decoding high-order modulation more complex and fragile, which leads to more error bits and, subsequently, more retransmissions that require energy consumption[11]. Although a modulation symbol in low-order On-Off Keying (OOK) modulation represents fewer bits, it is cheaper and more practical to use low-order, robust modulation instead of trying to improve the reliability of high-order modulations. Thus most OWC systems, such as OpenVLC and LiFi [6, 10, 12–23], switch from high-order to low-order modulation OOK, which is defined as primary modulation in the OWC standard IEEE 802.15.7 [24]. This allows for more robust transmission with a low bit error rate (BER), and therefore fewer retransmission.

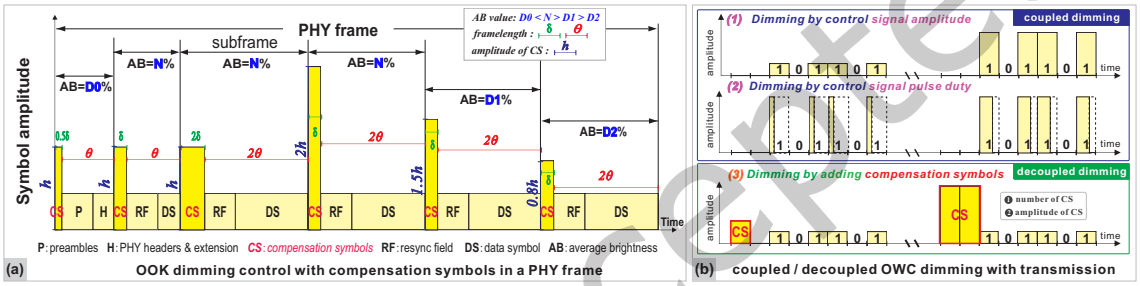

Fig. 1. (a) Illustration of OOK dimming control with compensation symbols (CS), redesigned from IEEE OWC standard [24]. A higher ratio of CS symbols in a subframe and higher CS symbol amplitude can both achieve higher average brightness (AB). (b) Core idea of LiFOD: utilizing CS as robust side-channel to denote more bits.

Challenge: When transmitting data via the optical spectrum, the brightness of LEDs may experience undesired flickers. Thus, in the OWC standard [24], compensation symbols (CS) are introduced in OOK modulation for smooth lighting and dimming control, while not affecting wireless communication. As shown in Figure 1 (a), in OOK-based OWC the entire PHY frame is split into multiple subframes. In each subframe, a continuous number of CS symbols proportional to the length of the subframe are inserted in front of the OOK symbols (`P`, `H`, `RF`, `DS` fields) to adjust average brightness (`AB`). However, authors in [25] observed that when more control is needed to achieve fine-grained dimming, there is less transmission opportunity for wireless communication and results in lower throughput. Moreover, CS symbols are solely used for dimming[16, 24], taking up transmission resources in the time domain, and limiting the data rate of OOK-based LiFi systems.

Motivation: Considering lighting, LED brightness may cause undesired flickers when transmitting data via the optical spectrum[8, 9, 24]. Meanwhile, dimming is essential to adjust light intensity for a variety of purposes, such as office or hallway lighting, sleeping, reading, or other activities, with benefits that include reduced eye strain, mood setting, and LED life extension. There are two key observations that motivate our approach to consider both smooth dimming and improved communication. **(1) Bit patterns** [26–28] occur in transmitted bit-streams. A bit pattern is a bit sequence (i.e., multiple continuous bits), that frequently occur in traffic during a historical period. **(2) Compensation symbols** have not been used for data transmission in OOK-based OWC networks. In related dimming research[29–32], approaches focus only on dimming itself without considering the potential for data transmission. However, we can use CS as a reliable **side-channel** to denote bit patterns

for improved throughput considering the significant symbol distances between CS and OOK symbols shown in Figure 1 (b).

In this paper, we propose **LiFOD** to exploit compensation symbols, which previously have been used solely for dimming, to carry data bits **firstly** for improved throughput in OOK-based OWC networks. In our work, compensation symbols are employed in both dimming controls and transmission. A bit pattern in a transmitted bitstream can be represented by one relocated CS symbol in the PHY subframe. The transmitter periodically conducts lightweight bit pattern discovery in parallel with modulation and notifies the receiver of the latest bit patterns via preambles.

Consequently, the network throughput improves remarkably due to improved data rate and decoding performance. **(1)** Data rate: CS symbols become data symbols without consuming transmission resources in the time domain. Moreover, each CS symbol carries more bits than an OOK symbol. **(2)** Decoding: CS symbols have a lower detection error rate than OOK symbols. Furthermore, the receiver decodes the CS symbol to its corresponding bit pattern directly instead of decoding multiple OOK symbols for that bit pattern, which reduces decoding error possibilities.

Our **contributions** are summarized as follows:

- We creatively exploit compensation symbols (CS symbols) to improve throughput. CS symbols were traditionally used only for dimming in OOK-based OWC systems. We explore bit pattern possibilities and propose a greedy mining algorithm to identify multiple bit patterns to maximize the overall throughput.
- To make the LiFOD practical for real-time communication, we explore the deep learning assisted bit pattern mining via the YOLO model. We creatively convert the bit stream into a 1D bar code with white and black rectangles and a 2D matrix with colored direction-specified slashes to enhance the feature of specific bit segments. The results demonstrate that our solution can achieve real-time bit pattern mining for LiFOD.
- We redesign non-flicker optical symbols (OOK and CS symbols) for smooth lighting and communication. This ensures the robust identification of symbol types in a changing environment. Initially, CSs are inserted continuously and proportionally into subframes for constant lighting. In our approach, CSs are relocated to discrete locations to denote bit patterns, which may introduce undesired flickers, however, we also design CS relocation schemes for stable lighting.
- We implement a LiFOD prototype on commercial devices and validate its lighting and communication performance in different transmission settings. Our comprehensive evaluation results demonstrate that **LiFOD** can achieve up to **400 Kbps** of throughput up to **6m** with fine-grained dimming, effectively **doubling** throughput at a longer range compared with SmartVLC on the SIGCOMM17 datatrace.

The paper is organized as follows: Section 2 introduces background and related work. Section 3 is system overview. Section 4 - Section 6 present how to utilize CS for both efficient communication and lighting from deep learning assisted *bit pattern mining* and *CSC coding* to *fine-grained dimming* and *decoding*. The implementation and performance evaluation are reported in Section 8-9. We conclude our work in Section 10.

2 BACKGROUND AND RELATED WORK

The single-color LED lamps[33, 34] are the most popular trend as a cost-effective choice for eco- and user-friendly residential lighting fixtures in our daily lives. Lighting and dimming are the **primary** functions of these LED lamps. Besides, photodiode (PD)-based OWC systems, such as OpenVLC and LiFi[6, 12–14, 14, 15, 35–37] with low-order modulations such as OOK, MPPM, and their varieties, treat wireless communication as **secondary** functions of these commercial LED lamps. To better delineate our research problem, we offer an introduction to Optical Wireless Communication (OWC) dimming functions and modulation below.

2.1 Dimming in OWC

Light dimming is defined as controlling a light source's perceived brightness to users. We classify the primary OWC dimming methods in the IEEE OWC standard[24] into two types, **coupled** or **decoupled** dimming with transmissions.

For **coupled dimming with transmission**, as shown in Figure 2, the control signals' amplitude has no impact on the time slots/carrier bandwidth of transmission while the control signals' pulse width influences the carrier's bandwidth. As observed in SmartVLC[38], a drawback of fine-grain coupled dimming control is the lower throughput that can be achieved because complex modulations, which allow fine-grained dimming control, waste transmission bandwidth and add more error bits. The researchers proposed Adaptive Multiple Pulse Position Modulation (AMPPM), which designs super symbols to generate more pulse width combinations for fine-grained dimming. However, AMPPM is still discrete step dimming with more modulation cost than the same-order OOK.

Decoupled dimming with transmission inserts compensation symbols (CS) into the data frame and sends constant brightness symbols of OOK modulation to adjust the average brightness of the light source. This treats data transmission and light dimming as two relatively individual modules with limited interaction. It has more robust communication and fine-grained dimming control while also providing the potential of using CS symbols to transmit extra data in comparison to coupled dimming methods. However, CS symbols take up time slots for data symbols compared with coupled dimming.

CS symbols have two ways to control a light source's average brightness shown in Figures 1 (a) and (b): (1) change the **number** of CS symbols in data frames and (2) adjust the **amplitude** of CS symbols. We can decrease the number of CS symbols as much as possible and adjust the amplitude of CS symbols for dimming to avoid taking up time slots for data transmission. Also, we can use CS symbols as a reliable side-channel to transmit specific data such as bit patterns. CS symbols will not waste time slots/carrier bandwidth anymore and even improve the communication performance.

2.2 Communication in OWC

In addition to lighting, it is also crucial to provide users with high-speed communication. Based on the receiver type and modulation, we classify OWC into two types:

(1) Camera-based OWC with high-order modulation. It is hard to achieve a sufficiently high data rate as the switch speed of the transmitters is too fast for the limited frequency response of the cameras as receivers[9, 39]. Rolling shutter cameras on smartphones offer a frequency response only up to a couple of **tens of kHz**, which is well below the needed value for high speed communication of **hundreds of kHz**.

To overcome the bottleneck of camera-based OWC systems, many researchers[1, 8, 9, 40] focus on designing high-order modulation schemes to improve throughput. In [8], authors proposed ColorBars to utilize Color Shift Keying (CSK) modulation to improve the data rate via Tri-LEDs. They achieved a data rate of up to **5.2 Kbps** on smartphones. Similarly, Yanbing et al. proposed Composite Amplitude-Shift Keying (CASK)[9] to improve the throughput of the Camera-based OWC system. CASK modulates data in a high-order way without a complex CSK constellation design. CASK achieves a data rate of up to **7 Kbps** by digitally controlling the On-Off states of several groups of LED chips.

These existing high-order modulations are high cost due to the necessity of specific devices and therefore cannot scale easily. For example, CSK modulation requires Tri-color LEDs as transmitters, which costs more than single color LEDs used in OOK and are quite unlikely to be deployed in real life[9]. CSK also needs a complicated and expensive receiver to precisely detect intensities of three colors: Red, Green, and Blue in the CIE color space chromaticity diagram[41].

(2) Photodiode-based OWC with primary modulation. Photodiodes (PD) are semiconductor P-N junction devices that convert the analog light signal into digital electrical current[42, 43]. PDs are single-pixel with a small surface area, which allows PDs to have a fast response time of sensing processing. This means the receiver can achieve a fast and robust symbol detection for high-speed communication. Most OWC systems, such as LiFi [12, 35] and OpenVLC[15, 36, 38, 44] adopt PDs as receivers for high-speed transmission and achieve a frequency response of a couple **hundreds of kHz**.

To suit a high-speed transmission frequency, PD-based OWC adopts primary and low-order modulations such as **OOK**. This occurs because it is non-trivial to demodulate higher-order optical symbols (e.g., 8-CASK, 32-CSK) at the PD-based clock speed of hundreds of kHz, due to reduced symbol distances compared to OOK symbols. Moreover, in poor optical channel conditions such as sunshine/underwater scenarios, the nonlinear effect of LED and short symbol distances makes them more complex and fragile with more error bits[11, 45–48]. Higher-order modulations will bring more error bits and need more retransmission for the required BER. Thus most popular OWC systems such as LiFi [12, 35] switch from high-order modulations to low-order modulation such as OOK for robust transmission with a low BER in changing environments with poor channel conditions. The latest version of OpenVLC[44] can achieve, on average, about **150 Kbps** at 4m under optical interference.

Our scope: We focus on the indoor OWC systems equipped with low-cost **PD** sensors and single-color commercial **LED** lamps, which are resilient lighting infrastructures. Our goal is to boost throughput and fine-grained dimming simultaneously without additional cost.

3 SYSTEM OVERVIEW

In our design, LiFOD system consists of commercial LED lamp based transmitter and PD-based receiver. The architecture diagram and workflows of LiFOD are shown in Figure 2.

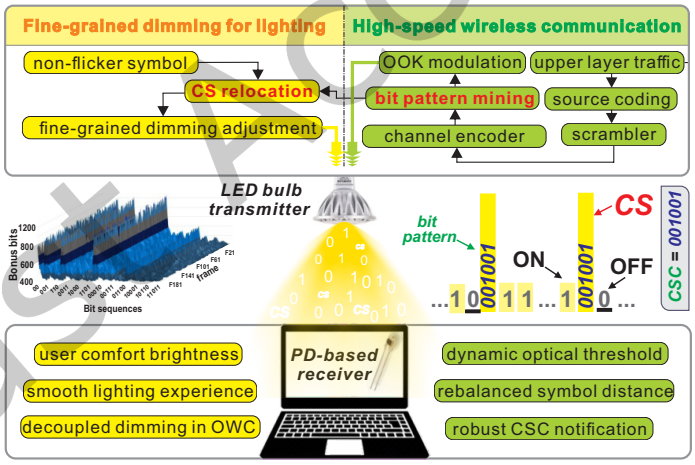

Fig. 2. System architecture and workflow of LiFOD.

(1) **Dimming workflow**: After a user turns on an LED lamp, they may start OWC. They can smoothly control the dimming level by adjusting the knob (actual physical knob or virtual knob on the IoT user interface). Manual adjustment is the most accessible and most fine-grained manner of dimming control as opposed to various communication-coupled dimming methods that can only provide digital and discrete step dimming[49, 50]. As shown in Figure 2, OOK symbols are constant brightness for data communication. In contrast, CS symbols are brightness-adjustable for fine-grained light dimming. Instead of the original continuous CS symbol insertion,

LiFOD uses discrete CS symbol relocation to denote bit patterns without impacting CS-based smooth dimming and the detection of OOK symbols for robust communication.

(2) **OWC workflow**: Modulation occurs when Internet data from upper layers is encoded as optical data symbols. There are three essential network modules before OWC modulations defined in the standard [24]: Source coding, Scrambler, and Channel coding. Our introduced module in LiFOD is a lightweight ***bit pattern mining*** module added after these three network modules, but before modulation. Although scrambling and channel coding has already occurred, there are still some frequently appearing bit sequences (e.g., "001001" in the illustration). These are bit pattern candidates. In a real-world trace, SIGCOMM 2017[51], as shown in the middle left in Figure 3, multiple bit sequences appear in high frequency and introduce bonus bits (i.e., we can add CS symbols to assist transmission and achieve a higher data rate than current standards).

(3) **Overview.** We encode p-length bit patterns into a Compensation Symbol Code (**CSC**) as shown in the middle right in Figure 2. Each instance of a CSC code increases transmission speed because more bits are transmitted if p>1. When allocating bits, we first check whether the next p bits match the predefined CSCs from our bit pattern discovery. If false, one bit is allocated to an OOK symbol as usual. On the contrary, we define it as a **hit** if the bits match the predefined CSCs. Instead of mapping only one bit to an OOK symbol, p bits are transmitted through a CS symbol. Once the receiver detects a CS symbol's existence, it inserts a p-bit CSC into the data stream. The receiver now can detect only one CS symbol that denotes p bits, instead of needing to detect p OOK symbols. Because (p-*1*) more bits (i.e., **bonus bits**) are transmitted when there is a hit and all symbol types/(ON/OFF/**CS**) are used for transmission, it is clear that the data rate of our system will increase.

4 GREEDY BIT PATTERN DISCOVERY

4.1 Mining Challenges

Throughput improvement introduced by bit patterns depends on the length of p and the hit rate in a given data frame. For example, as the length of a bit sequence increases, the probability of a hit decreases, and vice versa. There is a clear tradeoff between bit sequence length and hit probability. Moreover, as shown in Figure 2 and Figure 3, not only one bit sequence is likely to be a bit pattern. When one bit sequence is selected as a bit pattern, the bitstream will be split by this bit pattern. After one bit pattern is assigned, depending on which pattern is chosen, the resulting allocation of the data bits is wholly changed. The next challenge, is to decide which pattern will be selected as the next bit pattern. All options need to be explored based on the choice of the previous bit patterns.

An example is illustrated in Figure 4. Suppose the bit sequence "01" appears most often when allocating the bitstream "...1001010101110001...". Also, it offers the maximal bonus bits when compared with other potential bit sequences. In this case it is $(2-1)\times 5 = 5$ bonus bits. We may encode bit sequence "01" as one type of CSC. However, other bit sequences may also exist, such as "10", which often appears and brings the same level of bonus bits as "01", $(2-1)\times 5 = 5$. A challenge of LiFOD is deciding which bit sequence, in this case "01" or "10", should be selected as the bit pattern. **(1)** If we choose "01" as the bit pattern, the bit stream will be split into three bit segments: "...10", "...1100..." and "...". **(2)** If choosing "10", the bit stream will be split into four bit segments: "...", "0", "11", and "001...".

Additional bit sequences also frequently appear in the split bit segments produced after the first round of bit pattern selection. These sequences can be chosen as another bit pattern to further speed up the data rate. However, the bit pattern selected for a specific round impacts the bit pattern choice for the next round, and previously discovered bit pattern candidates in earlier rounds may not be candidates anymore. When choosing bit patterns, we need to consider the total bonus bit performance of all chosen bit patterns of all rounds.

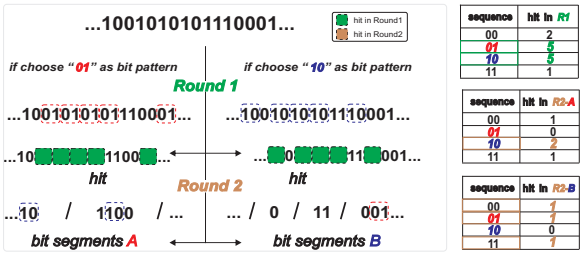

Fig. 3. Bit pattern candidates change in next round.

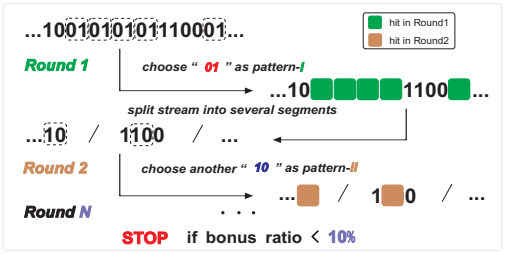

Fig. 4. The illustration of multiple rounds mining.

4.2 Identify Patterns Greedily

To address the problem above, we execute bit pattern mining in multiple rounds shown in Figure 4. The bit pattern for each round will be selected as different types of CSCs. After several rounds of mining, there will be less opportunity to find bit patterns because bitstreams have already been split into short-length segments. Consequently, any obtained bonus bits will decrease as the number of rounds increases. Furthermore, if there are too many types of CSCs, the compensation symbol design for modulation will be more complicated and therefore increase the error rate of demodulation. Therefore, the choice to continue bit pattern mining is a tradeoff between increased data rate and error rate. The number of rounds we run for bit pattern mining depends on the bonus ratio for each round. The bonus ratio is defined as the ratio of bonus bits introduced by CSC for a specific round to bit numbers of the entire data frame. When the bonus ratio is less than **10%**, bit pattern mining stops at that round, and any previously mined bit patterns are chosen as CSCs.

According to analysis above, we design a lightweight greedy algorithm to explore bit patterns and summarize multiple rounds algorithm in Algorithm 1. The goal is to bring the maximum number of bonus bits possible in each mining round locally and obtain the maximum bonus bits of all mining rounds globally.

Based on our experimental results, we've determined that with a bit sequence length larger than six bits the total number of bonus bits we gain starts to fall, and therefore we search for bit sequences whose length is up to 6 as bits long. The number of bit sequences possible is $\sum_{i=2}^{6} 2^i = 124$. We scan each of them in the frame, count hit number, and calculate bonus bits. We then choose the bit sequence with the most bonus bits as the bit pattern at that mining round. We calculate the bonus ratio of the bit pattern for each round and compare it with the 10% threshold. If the bonus bit ratio less than the threshold, mining will stop at that round.

4.3 Ablation Study of Bit Pattern

Real-world Daily Data-trace. The OWC backhaul is connected with the Internet[35, 52, 53]. We conduct CSC code abstraction based on two sets of real-world wireless traffic data from the (1) SIGCOMM 2017 trace [51], which is the recorded wireless network activities at the SIGCOMM 2017. (2) Another trace is from CAIDA 2019 [54], which collects the daily network traffic of a city in the US. These data packets are scrambled and encoded with the convolutional encoder specified in the IEEE 802.11 standards.

4.3.1 Bonus Bits Distribution and Potentials. Figure 5 shows heat maps of our bit pattern mining results in Round 1 and 2 among different frames from our two traces. There are more bit pattern candidates in Round 1 (i.e., six strongly highlighted columns). In Round 2, there are fewer bit pattern candidates (i.e., two significant highlighted columns) and the bonus bits in Round 1 are much more significant than Round 2. It implies that there are abundant known bits in the first round of mining used because of the high probability of having a hit on the CSCs. In high-order rounds, opportunities to use CSCs are few.

Algorithm 1: Greedy based Bit Pattern Mining

Input: A bit stream of a PHY frame *Frame*
Output: Mutiple bit pattern: CSC-I, CSC-II, ...

```
1  R ← 1;  // round number
2  set1 ← bit sequences ;
3  set2 ← bit segments;
4  N ← size (set1);
5  M ← size (set2);
6  n ← 0; //index of set1
7  m ← 0; //index of set2
8  S  //bit segment
9  C  //check area in S
10 P //bit sequences in set1
11 while bonus_ratio > 10% do
12     bonus ← 0;
13     R++;
14     S, C, P ← empty string;
15     while  m < M do
16         S ← set2[m++];
17         L ← size(S);
18         while  n < N do
19             P ← set1[n++];
20             k ← size(P) ;
21             i ← 0;
22             while i < L - k do
23                 C ← bits from S[i] to S[i+k];
24                 if C == P then
25                     bonus[n]+ (k-1);
26                     i ← i + k;
27                 else
28                     i ← i + 1;
29     decide CSC-R;
30     strip CSC-R from set2;
```

4.3.2 Tricks of CSC Decision in a Round. In general, the decision to choose a particular bit pattern candidate as a CSC code for each round depends on their bonus bits. However, if two bit pattern candidates have identical bonus bits, as occurs in Round 1 of the SIGCOMM17 trace shown at the top in Figure 6, we choose the longer bit pattern candidate "000000" as the bit pattern even if other bit pattern candidates have the same bonus ratio performance for that round. The reason is that when two or more bit pattern candidates have identical bonus bits the longer one will make the bit segments shorter after splitting the longer bit pattern to achieve as fewer mining rounds as possible. Thus, there will be less hits in the next round which means there will be more CSC-I and less CSC-II.

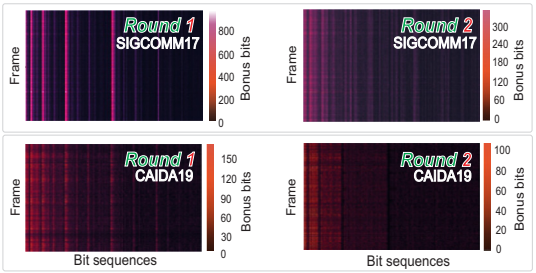

Fig. 5. Bonus bit heat maps for two rounds mining

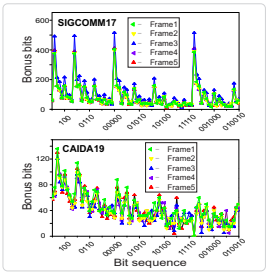

Fig. 6. CSC decision tricks

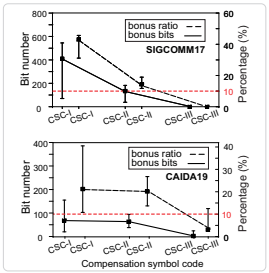

Fig. 7. Considerable bonus.

4.3.3 Two CSC with Considerable Exta Data. Figure 7 shows that in Round 1 of mining, more than 40% of all bits are transmitted as bonus bits through CSC-I of the SIGCOMM17 trace. The CAIDA19 trace, also achieves a bonus ratio of more than 20% for CSC-I. As the number of mining rounds increases, a lower percent of bonus bits can be used, however, the bonus ratio is still above 10% Round 2 in the SIGCOMM17 trace. The bonus ratio in Round 2 for the CAIDA19 trace remains near 20%. In Round 3 of mining for both traces, the bonus ratio falls below the threshold of **10%**, and subsequently, the mining stops after Round 3.

Finally, we choose **two CSCs** (CSC-I and CSC-II) that will be used for transmission. The total bonus ratio of the two rounds of mining on two real-world traces is, combined, more than **40%**. Although the transmission rate benefits less directly from bonus bits when utilizing CSC-II, it still provides decoding benefits from the known bits represented by CSC-II. Overall, the more bits represented by CS symbols, the fewer opportunities for the false detection for OOK symbols.

4.3.4 Delay and Overhead Measurement. We analysis and measure the overhead of bit pattern mining based on real-world data traces SIGCOMM17 and CAIDA19. The results of execution time and memory overhead of our greedy bit pattern mining algorithm are shown in Table 1. The bit pattern mining process for SIGCOMM 17 and CAIDA 19 consumes **0.78 s** and **0.37 s** in average. The computation cost of our pattern mining for SIGCOMM 17 and CAIDA 19 data-traces are both **144 MiB** of memory in average.

Two real-world data trace	Execution Time (s)									Memory Overhead (MiB)								
	Round 1			Round 2			Total			Round 1			Round 2			Total		
	min	max	ave	min	max	ave	min	max	ave	min	max	ave	min	max	ave	min	max	ave
SIGCOMM 17	0.44	0.87	0.61	0.12	0.24	0.17	0.56	1.67	**0.78**	72	72	72	72	72	72	144	144	**144**
CAIDA 19	0.11	0.38	0.22	0.07	0.25	0.15	0.18	0.63	**0.37**	72	72	72	72	72	72	144	144	**144**

Table 1. Delay and overhead measurement of bit pattern mining on two real-world data traces.

5 FINE-GRAINED DIMMING VIA CS

5.1 Non-flicker Symbol Design

Flicker is the temporal modulation of lighting perceivable by the human eye, which can negatively affect a user's lighting experience. The maximum flickering time period (MFTP) is the maximum time period over which the light intensity can be changed and not sensed by human eyes. Thus any brightness changes over periods longer than MFTP must be avoided (i.e., significant low frequency brightness changes cause flickers and should be mitigated)[24].

In the current standard, OFF/ON and CS symbols have different amplitudes, and as shown in Figure 8, CS-I and CS-II also have different amplitudes. The random distribution of CSCs encoded by LiFOD that appear in PHY

frames at low frequencies causes significant flickering. To address this, our flicker-mitigation solution is inspired by Manchester coding [24], where each symbol is extended to include itself and its complementary symbol. This guarantees that any significant brightness changes will appear too fast to be sensed by human eyes.

There are three amplitude scales in the new symbol design: B0, B1, and B2 (brightness: B0 < B1 < B2) for OFF, ON, CS-I, and CS-II symbols instead of four brightness amplitudes in the original symbol design. Symbol **OFF** is designed as **B0+B1**. In the first half of a symbol's duration, it has an amplitude of B0. In the second half of a symbol's duration, it has an amplitude of B1. Similarly, symbol **ON** is designed as **B1+B0**. And we design **CS-I** as **B2+B0**, while **CS-II** is **B0+B2**. Our newly designed symbols only need two thresholds rather than three for demodulation, decreasing the complexity and load of symbol detection. This increases the symbol distance and decoding robustness further. Additionally, CS-I and CS-II have the same brightness in our non-flicker symbol design, which further reduces the flickering possibility compared to the standard symbol design.

Note that there exists more CS-I symbols than CS-II symbols. It is easier for the receiver to distinguish the amplitude difference between B2 and B0 than between B1 and B0. Suppose a symbol has an amplitude of B2 in the first half of symbol duration. In this case, the symbol will be decoded as one CS-I symbol directly without estimating the amplitude of the second half symbol duration. That is why we design the CS-I symbol as B2+B0 instead of B0+B2. This design decreases the detection error rate (DER) of the CS-I symbol, which carries more data than the CS-II symbol. Finally, this benefits total throughput and BER performance.

5.2 Compensation Symbols Relocation

Fine-grained dimming control. LiFOD consists of two commercial LED lamps that are controlled synchronously shown in Figure 8 (b). The transmitter sends out OOK symbols via LED1 and sends out compensation symbols via LED1 and LED2 together. LED1's brightness is set by the user and fixed before OWC begins. Users can continuously adjust LED2 by the dimmer knob to provide the additional brightness of (B2-B1, i.e., ΔB) to increase or decrease the average brightness (**AB**) without impacting optical symbol detection. This saves transmission bandwidth and does not affect symbol decoding. The number of CS symbols is proportional to each frame's length to guarantee the same AB between frames. This mitigates **inter-frame** flickers and keeps constant brightness, even after an updated dimming is set.

Random CSC Locations and Numbers. There are subframes in each frame. Currently, compensation symbols are continuously inserted into subframes for dimming control in the IEEE OWC standard[24]. However, these are incapable of denoting the bit patterns that may appear discretely in the bitstream of one frame for transmission. Moreover, the hit numbers of CSC-I and CSC-II are not always the same in subframes, even though different subframes should have the same brightness to reduce **intra-frame** flickers. This means each subframe should have an equal proportion of CS-I and CS-II symbols.

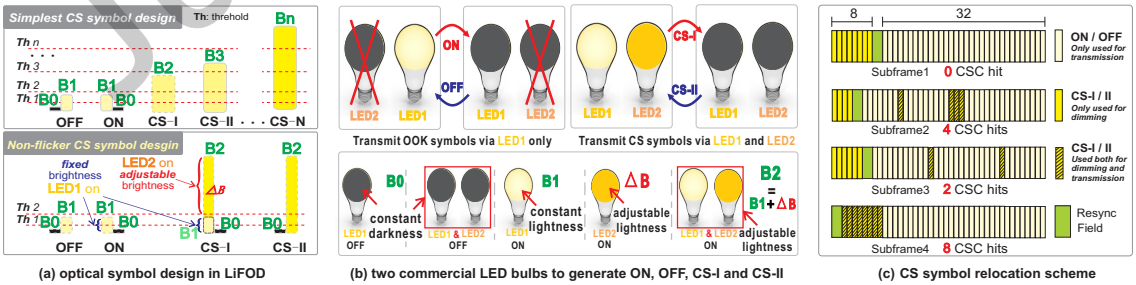

Fig. 8. Optical symbol design with fine-grained dimming and CS relocation scheme illustration in LiFOD.

Random CSC Locations and Numbers. There are subframes in each frame. Currently, compensation symbols are continuously inserted into subframes for dimming control in the IEEE OWC standard[24]. However, these are incapable of denoting the bit patterns that may appear discretely in the bitstream of one frame for transmission. Moreover, the hit numbers of CSC-I and CSC-II are not always the same in subframes, even though different subframes should have the same brightness to reduce **intra-frame** flickers. This means each subframe should have an equal proportion of CS-I and CS-II symbols.

CS Relocation. In Figure 8 (c), there are 40 OOK and CS symbols in each subframe. We set $\frac{1}{5}$ of the symbols (i.e., 8 CS symbols) for dimming to keep a constant AB of the subframe. There are 8 CS symbols at the beginning of each subframe initially. If there is a CSC-I/II in the subframe, we put one CS-I/II symbol in that location. These picked CS-I/II symbols are used both for dimming and assisting transmission. The left redundant CS-I/CS-II symbols at the front part of the subframe are only used for dimming. The CS symbols only used for dimming are separated by the resync field (RF) in Figure 1 with symbols used for transmission (OOK and picked CS symbols). We only decode the symbols after the RF field. Compared with the original, continuous CS symbols, CS relocation provides the potential to create robust side-channels for data transmission and mitigates the flickering possibility further as an unintentional benefit while keep constant brightness.

6 ROBUST DECODING OF CS

6.1 Dynamic Optical Threshold

As shown in Figure 8 (a), the receiver checks grayscales of two parts in one received symbol to identify its symbol type by its grayscale threshold. In LiFOD's non-flicker design, there are three brightness levels B0, B1, and B2. The receiver distinguishes them based on grayscale thresholds informed by a preamble from the transmitter.

However, as shown in Figure 9, a received grayscale is not identical to the one transmitted by the transmitter under four different dimming levels (i.e., B2's incremental brightness). The received grayscale of different brightness may overlap with others, and B2 in different dimming settings can influence the perceived brightness of B0, B1 due to their continuous distribution in the PHY frame. To identify an optical symbol's type with varying brightness, the receiver should be informed of dynamic thresholds among B0, B1 and B2 via a **preambles** from the transmitter. Grayscale thresholds are measured and calculated based on short training symbols in the preamble field. The threshold values are dynamically adjusted based on the measurement informed by the preamble.

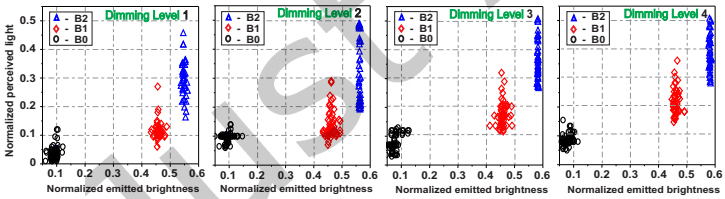

Fig. 9. Grayscale diagram of B0, B1, B2 on 4 incremental dimming levels.

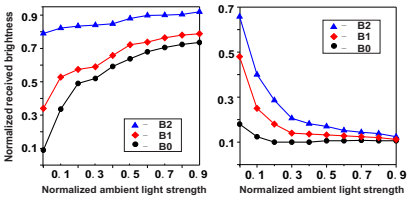

Fig. 10. Influence of two factors.

6.2 Rebalanced Magnitude Distance

In addition to our dynamic threshold measurement with preambles for different dimming settings in varying environments, we also need to combat any environmental influences. When an optical signal radiates away from its transmitting light source, the signal spreads out in different directions. Parts of spreading light beams reflect off objects and arrive at receiving light sensors from different paths. Consequently, different ambient light brightness will impact detection of original optical symbols.

If the ambient light is weak, the brightness of B1 or B2 will dominate the receiver's sensed intensity. When ambient light gets stronger, the ambient light will dominate the received brightness and the brightness of B0, B1, and B2 will have a similar high grayscale level, as shown in the left of Figure 10. The same case happens when the transmission distance increases. When the transmission distance between transmitter and receiver becomes larger, ambient light will dominate the receiver's brightness as well, as shown in the right of Figure 10. The intensity of B0, B1, and B2 will have a similar low grayscale level.

These two factors significantly cause the perceived magnitude of brightness transmitted to be harder to distinguish from one another, and therefore, the received symbol is not identical to the transmitted optical symbol. We need to estimate the optical channel response using the **preamble** to further conduct equalization to eliminate the influence of ambient light and transmission distance.

Suppose optical channel response O is $H(O)$ and the transmitted brightness is $\boldsymbol{b}$. The received brightness is

$$b' = H(O)b \tag{1}$$

A sequence of known brightness values in the preamble, $\boldsymbol{S}$, are transmitted to help estimate channel response. $H(O)$ is estimated as

$$\hat{H}(O) = \frac{S'}{S} \tag{2}$$

where received brightness $\boldsymbol{S'}$ includes an ambient light and transmission distance factor. The $\hat{H}(O)$ is not equal to $H(O)$ due to other noises such as the temperature variation and noise figures at receiver, but it is still well estimated because $\boldsymbol{S}$ is known at receiver.

The subsequent brightness magnitudes, $\boldsymbol{x}$, B0, B1 or B2, are finally estimated by multiplying received brightness $\boldsymbol{x'}$ with the multiplicative inverse of the estimated optical response of channel $\hat{H}(O)$:

$$\hat{x} = \frac{x'}{\hat{H}(O)} \tag{3}$$

6.3 Robust CSC Notification

Preambles are used in LiFOD to notify the receiver of the CSC codes used in our system. The IEEE 802.15.7 standard [24] defines the format of the Physical Protocol Data Unit (PPDU). The PHY frame consists of a synchronization header (SHR), a PHY header (PHR), and Physical Service Data Unit (PSDU). The SHR contains the preamble field. CSC-I and CSC-II are prepended to the data packet in the preamble field to inform the receiver of the bit patterns being used. The receiver stores CSC codes and understands that they are specified for CS-I and CS-II symbols separately.

When the receiver estimates the transmitted brightness magnitude by dividing the estimated optical response of channel $\hat{H}(O)$, the absolute magnitude change on a symbol with a lower magnitude is lower than that on a higher magnitude symbol, as shown in Figure 11. For example, if the estimation is that a received symbol should be magnified by 20%. The absolute magnitude changes of symbols are different. Low magnitude symbols have a minor error margin, while magnitude errors of high magnitude symbols are scattered in a broader range than that of low magnitude symbols. Because LiFOD only adopts three brightness magnitudes (B0, B1, B2) in symbol design, the equalization can successfully eliminate the influence of the varying environment.

When using compensation symbols for transmission, the dimming will not impact the ON/OFF symbol identification due to the smaller magnitude estimation error margin of B0 and B1 in OOK symbols than B0 and B2 in CS symbols. Nevertheless, suppose there are too many types of CS symbols. In that case, the decoding performance of CS symbols with a higher magnitude will get worse due to the broader estimation error margin. LiFOD uses two CS symbols with B0 and B2 brightness magnitudes, ensuring robust CSC notification.

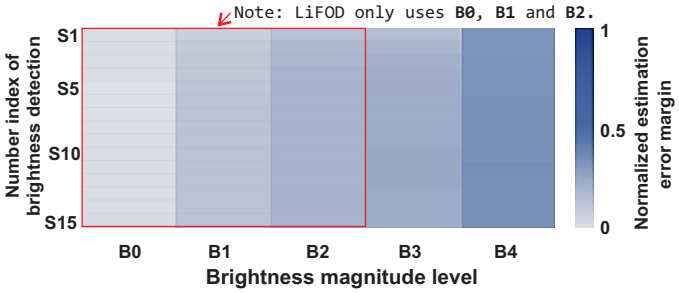

Fig. 11. The normalized magnitude estimation error margin of 15 detections in varying environment.

7 SPEED UP BIT PATTERN MINING

As reported in Section 5, there are bit patterns in Internet traffic that can be transmitted via CS symbols for an improved data rate. However, the greedy bit pattern mining has a non-trivial discovery latency and overhead. To make our LiFOD practical in the real-world, we explore CNN based real-time bit pattern mining.

7.1 Practical Requirements for BP Mining

Mining Latency Requirement. The indoor LiFi may support real-time applications, such as video streaming, AR and VR, which require the processing of PHY frame in a real-time manner. Real-time video streaming means the update video frame rate should be faster than the frequency response of human eyes (i.e., 60 Hz). Thus, the latency of bit pattern mining should be less than the video frame duration (e.g., **16.7 ms** when the video frame fresh rate is set at 60 Hz). The above greedy bit pattern mining requires an average time of 1.15 s (i.e., **1150 ms**) for two rounds cannot meet this requirement.

Frame-specified Bit Patterns. It has been demonstrated there are bonus bits for the two real-world internet traffic datasets above. However, the bit patterns may vary with time or different applications and the bit patterns in each PHY frame may be totally different. Thus, the bit pattern should be mined for each PHY frame. Therefore, real-time bit pattern mining is required to make LiFOD practical for real-world applications.

7.2 YOLO based BP Mining

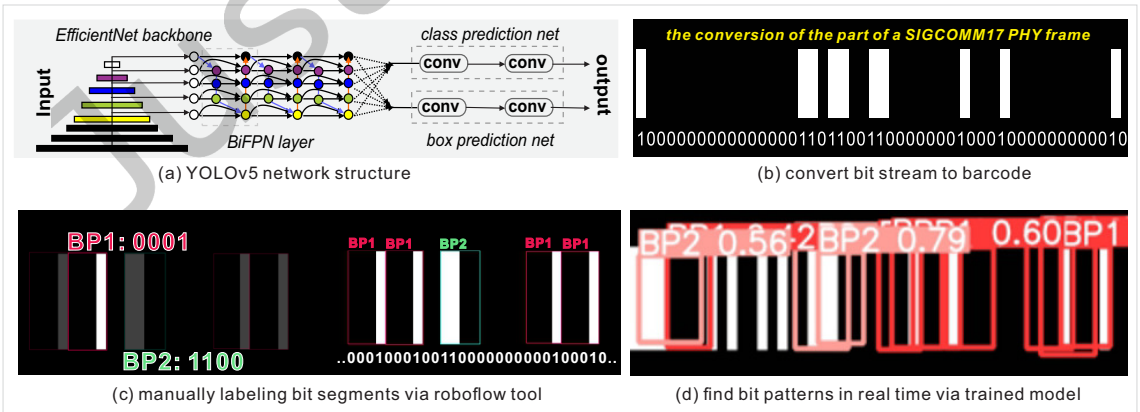

Fig. 12. YOLO based bit pattern mining details and three main steps.

7.2.1 Core Idea. The time complexity of greedy bit pattern mining in Algorithm 1 is $\mathbf{O}(n^3)$, which counts the appearance of each bit segment in the PHY frame in a linear manner and scans the PHY frame numerous times. Can we discover the different bit segments in parallel at once and then count their appearances for the bit pattern decision?

Computer vision applications such as real-time vehicle tracking and face recognition require the detection of multiple objects in real-time. Thanks to the well-trained offline models, we can achieve real-time online objective detection. With such inspiration, we can convert bit streams of a PHY frame into images and train CNN models to learn the features of different bit segments offline. Finally, we can detect multiple bit segments at the same time in a real-time manner that is similar to computer vision multiple object detection.

Because of their fast inference and excellent accuracy, YOLO (You Only Look Once) models are often used for object detection[21, 55]. As illustrated in Figure 12 (a), the network topology of YOLOv5[56] consists of EfficientNet backbone structure and BiFPN (Bi-directional Feature Pyramid Network) layers to extract object characteristics effectively. Then, as output, these features are sent through prediction networks for both the objective's class and the position of boxes. Therefore, we adopt YOLOv5 in the following real-time bit pattern mining.

7.2.2 Three Steps. There are three main steps in YOLO based bit pattern mining. We elaborate below.

(1) Convert Bit Stream into BarCode Image. First, we need to convert the raw bit stream into a BarCode image that contains the features of different bit segments via the OpenCV tool. As shown in Figure 12 (b), the bit '**1**' is denoted as a white bar, while the bit '**0**' is denoted as a black bar. Then, the bit stream is converted to continuous white and black bars with varied width related to the bit stream. Therefore, the features of different bit segments are encoded into the converted BarCode images. This processing enhances the pattern features from 0 dimension bit stream into 2D images, which helps for the following bit pattern mining.

(2) Label Bit Segments for Offline Learning. Then, we use the roboflow tool to label the bit segments manually for YOLO model offline training. As learned in greedy bit pattern mining, we know that the length of bit segments is proper to set in the range of (2, 3, 4, 5, 6). There are [00, 01, 10, 11, 000, 001, 010, 011, 100, ..., 00000, 000001, ..., 111110, 111111], totally 124 types of bit segments. Given an example of manual labeling, we can manually label bit segment '0001' as BP1 (one of the bit pattern candidate) and bit segment '1100' as BP2 (another bit pattern candidate) in the converted BarCode images as the dataset for YOLO model training, as shown in Figure 12 (c). Then we can use the offline trained model to predict the appearance of BP1 and BP2 including their location and times in the given bit stream in real time. Even multiple bit pattern candidate can be found without the significant increasing of the discovery time.

(3) Find Bit Patterns in Real Time. Using the trained YOLO model with a manually labeled dataset, we can achieve the real-time prediction of multiple objects (i.e., different bit segments) with their appearance locations and times with high confidence, as shown in Figure 12 (d). Although there are some overlaps of recognized bit segments, which is different from greedy bit pattern mining, the appearance times of the specific bit segment can still reflect the possibility the bit segment's ability to bring the bonus bits. Besides, the detection of different bit segments is processed in real time (i.e., <**16.7** ms) thanks to the well offline-trained YOLOv5 model. Finally, we can pick the two most frequently appeared bit segments as bit patterns for further CSC modulation.

7.3 Optimizing with 2D Embedding

The limitation of 1D embedding. However, CNN image processing requires a square image with the same length and width of pixels. The converted 1D bar code of a long bit stream only appears in a small portion of a square image, which causes a non-trivial detection performance drop due to the fewer pixels to present the feature of a specific bit pattern candidate, as shown in Figure 13 (b). To suit CNN processing, we optimize the bit stream conversion by embedding the long bit stream row by row into a bit matrix, as shown in Figure 13 (a).

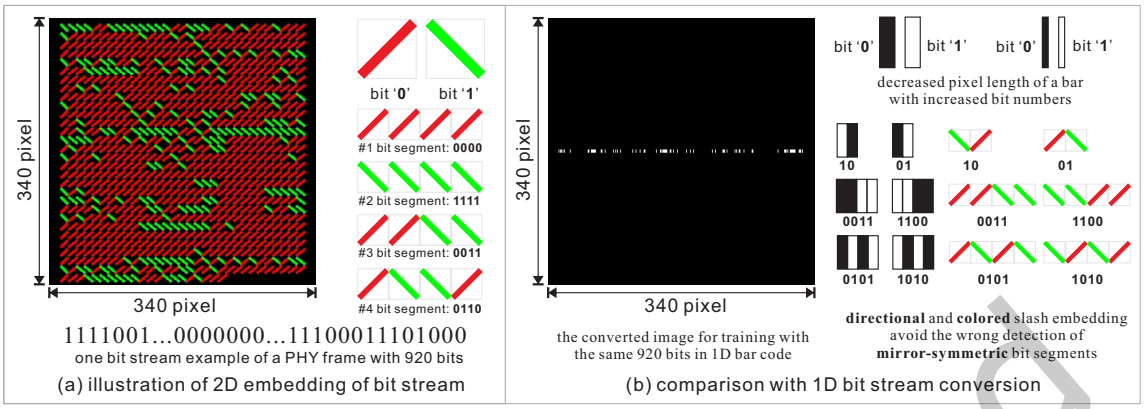

Fig. 13. Using 2D embedding of bit streams instead of 1D BarCode for mining improvement.

Avoidance of Wrong Detection. Besides the 2D embedding, we also enhance the feature of a specific bit segment by presenting bit '0' as the red slash with right phase and bit '1' as the green slash with left phase, as illustrated in Figure 13 (a). There are benefits of this redesign: (1) the generated pattern for specific bit segments are more significant compared with previous white and black rectangles, (2) the generated patterns avoid the confusion for the mirror-symmetric bit segments such as '0011' and '1100' or '01' and '10'. These mirror-symmetric bit segments have different patterns in our 2D embedding, which can allow us to conduct dataset augmentation by flipping or rotation without confusion for YOLO model, as shown in Figure 13 (b).

Rough but Fast BP Mining. As the split short bit streams row by row, the possibility of long bit segments' appearance may decrease. Instead of previous 6 bit length in bit pattern mining, we can only set bit segments within 4 bits. Besides, we can use one-round rough bit pattern mining in one 2D embedding PHY frame image based on their appearance times. Instead of only 2 bit patterns in the previous fine-grained but relatively slow bit pattern algorithm, we can choose multiple bit patterns combined with redesigned optical compensation symbols to transmit more bonus bits in real time. Some examples are shown in Figure 19. This optimized 2D embedding can provide a tradeoff solution between bonus bits and mining speed.

8 IMPLEMENTATION

In this section, we present our prototype of LiFOD including hardware and software at both transmitter and receiver.

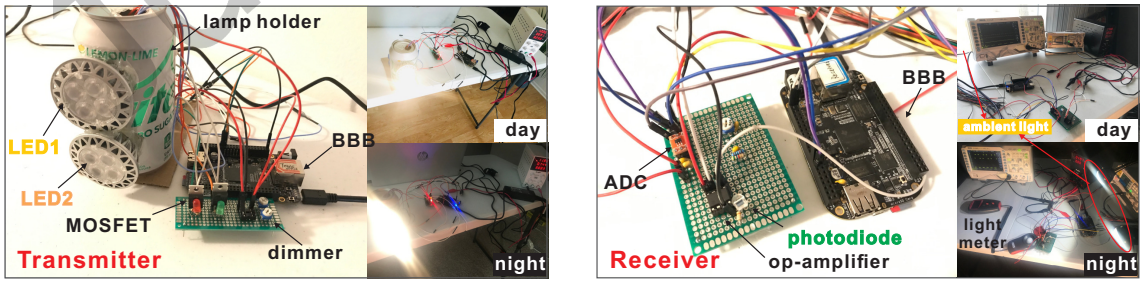

Fig. 14. LiFOD prototype: transmitter, receiver and experiment scenarios in day and night.

8.1 Hardware

Transmitter. Our LiFOD transmitter consists of several commercial components: two regular LED lamps (LED1, LED2), and MOSFET and BeagleBone Black (BBB) boards[57, 58]. LED1 is used to generate constant-brightness OOK symbols, LED1 and LED2 are used to generate variable brightness CS symbols as introduced in Section 5.2. They are controlled uniformly by the BBB board. Because BBB can only provide 3.3V control signals, which cannot drive high-power LEDs, we use a MOSFET transistor as a fast switch to drive the high-power LEDs (12V). To provide variable and fine-grained dimming, we wired two potentiometers as the dimmer knob between the DC power with the LED lamps' positive leads (i.e., adjustable resistor). The potentiometer for LED 1 is set fixed at the initialization. The poentiometer for LED 2 can be adjusted by user during usage. We removed the AC-DC converter in our daily LED lamp, which affects the ON-OFF switching speed significantly. The circuit diagram of LiFOD transmitter is shown in Figure 15 (a).

Receiver. The LiFOD receiver prototype has three main components: analog-digital converter (ADC), operational amplifier (OPA), and the photodiode (PD). The light is sensed by the PD to convert light signal to a small current and amplified by OPA. Finally, analog values are converted to digital values in SPI data format and then processed to estimate analog light intensities for symbol decoding. The driving circuit can be fully powered and controlled by the BBB. The circuit diagram of the LiFOD receiver is shown in Figure 15 (b).

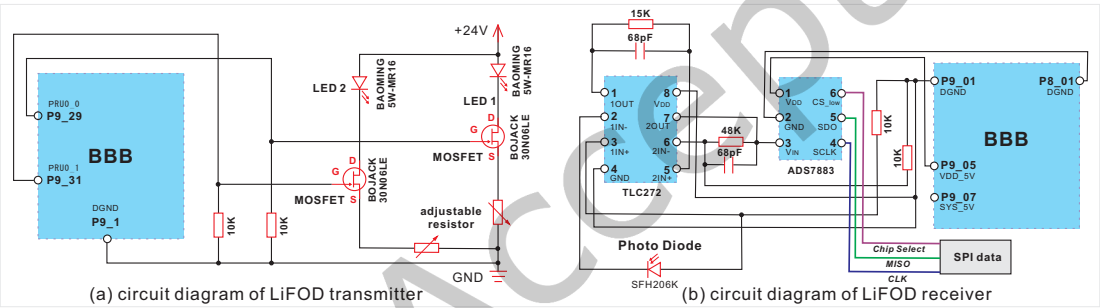

Fig. 15. The circuit diagram for LiFOD transmitter and receiver.

System cost. The system cost of LiFOD is shown in Table 2. The Beaglebone Black board ($80) in our prototype can be fully replaced with Beaglebone pocket($37), which is cheaper. Thus, totally including transmitter and receiver, the LiFOD system costs less than $100.

Component	Brand/Model/Type	Unit Price (USD)
LED Bulb	BAOMING-5W-MR16	**4.2**
MOSFET	BOJACK-30N06LE	**0.7**
Photodiode	OSRAM SFH206K	**1.4**
Op-amplifier	Todiys-TLC272	**2.4**
ADC	TI-ADS7883	**3.2**
potentiometer	HUAREW-PTM15	**0.1**
BBB board	Beaglebone-Black or Pocket	**80** or **37**

Table 2. Price table and system cost of LiFOD.

8.2 Software

There are two main tasks on the software side: (1) send out optical symbols at high speed from the transmitter; (2) demodulate received optical symbols at high speed with reliability on the receiver. We use low-cost BBB

platforms. Ideally, the PRU of BBB can achieve high-frequency modulation and demodulation at the *200MHz* level. But due to significant distortion of light signals generated by commercial LED lamps at such high transmission frequencies, in this work, we set the transmission frequency at *hundreds KHz* level, which is the same as the state-of-art SmartVLC or OpenVLC. Other software modules, such as our lightweight bit pattern mining and CS relocation, as shown in Figure 3 are run on the BBB as firmware to provide services among the PHY layers and upper layers.

9 EVALUATION

9.1 Setup

We choose two real-world datasets SIGCOMM17 and CAIDA19, to simulate user's daily Internet traffic. **(2) Transmission frequency.** We set the transmission frequency to be lower than 200KHz. **(3) Sampling rate.** To better detect the optical symbol shape, we set the ADC sampling rate to 1.2MHz, six times of transmission frequency. **(4) Ambient light setting.** Based on real-world scenarios, we conduct experiments in a 4 x 8 m^2 living room in the day and night scenarios. **(5) Dimming setting.** We set the dimming level by adjusting the dimmer knob neatly and using a light meter to measure its granularity.

9.2 Performance

9.2.1 *Lighting and Dimming Performance.*

Fine-grained dimming: The brightness of LiFOD can be manually adjusted to any continuous setting. We evaluate ten incremental dimming levels at different distances, as shown in Figure 16 (a). The dimming range is from 0 lux to 450 lux, which meets the office lighting requirement from U.S. General Services Administration [59]. In the different dimming setting index, the brightness sensed by the user increases depending on the day or night scenarios. The experiment results prove that the dimming function works well.

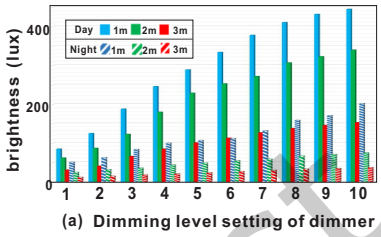

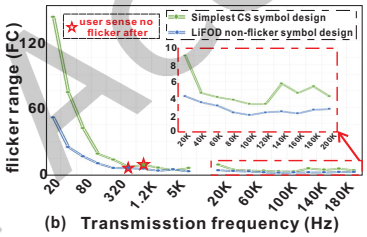

Total Scores at 10 Dimming Settings		User A		User B		User C		Average	
		FLK	LIT	FLK	LIT	FLK	LIT	FLK	LIT
View	direct view	9	10	10	10	10	10	9.7	10
	side view	10	8	10	10	10	9	10	9
Distance	1 m	8	9	10	9	9	9	9	9
	3 m	10	8	10	10	10	9	10	9
	5 m	10	8	10	10	10	9	10	9

Flickering (**FLK**) and lighting (**LIT**) scores for 10 dimming setting at 100 KHz transmission frequency. If one senses no flickers or has comfortable lighting at specific setting, the score is 1, otherwise 0. The score value in each cell is the sum of 10 settings.

(c) Users' perception scores

Fig. 16. Evaluation of fine-grained dimming and non-flicker performance. Users' perception scores of flickering (FLK) and lighting (LIT) for 10 dimming setting at 100 KHz transmission frequency. If one senses no flickers or has comfortable lighting at specific setting, the score is 1, otherwise 0. The score value in each cell is the sum of 10 settings.

Non-flicker performance: We measure the non-flicker performance with the light meter via the photometric quality, which measures the foot candle (FC) value range from its minimum to maximum values. The more extensive range of FC values, the more flickering possibility. When the transmission frequency increases, the flicker possibilities reduce for the two optical symbol designs. Figure 16 (b) shows that users sense no flickers since the transmission frequency for LiFOD's non-flicker symbols are lower than the original optical symbols. Due to the unexpected low frequency of CS symbols, LiFOD's non-flicker symbols will provide more smooth lighting without flickering than the original symbol design, even at a very high transmission frequency such as 200KHz. Results show that our flicker-mitigation solution addresses the flicker well.

We also investigate users' perception of flickering and comfortableness of lighting, as shown in Figure 16 (c). Three volunteers are invited to experience the lighting function of LiFOD. Each user scores their user experience

for 10 dimming settings in different conditions such as facing directly or indirectly, at different distances to LED lamp. The results show all users have good experience with comfortable and stable lighting perception.

9.2.2 Communication Performance.

In this section, we evaluate the throughput performance of LiFOD in three aspects: (1) throughput vs. transmission frequency and distance; (2) throughput vs. incident angle and position; (3) throughput comparison with the state-of-art OWC schemes considering fine-grained dimming and high-speed communication simultaneously.

(1) Impact of transmission frequency and distance.

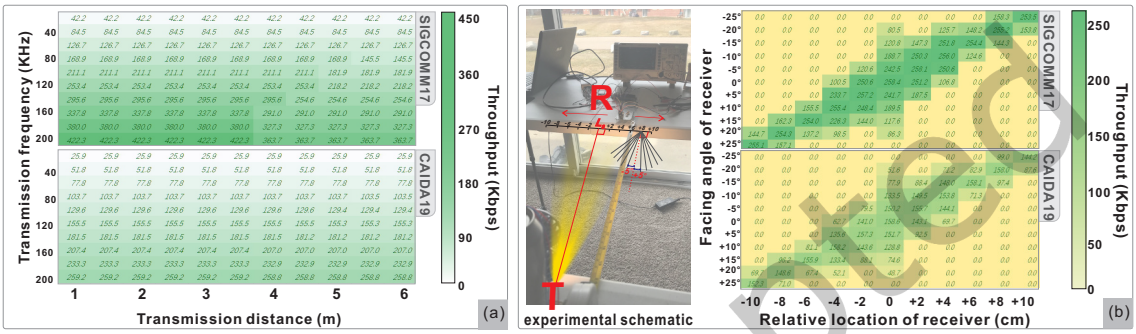

Fig. 17. Throughput performance evaluation of LiFOD. (a) Throughput vs. distance and frequency, and (b) Throughput vs. incidence angle and position.

We first evaluate throughput performance at different transmission frequencies and distances based on two real-world data traces. As shown in Figure 17 (a), the throughputs increase significantly as transmission frequency increases at the same distance setting. Although increasing distance will cause the throughput decline, it decreases less noticeably due to our robust symbol detection. Due to the higher bonus bits introduced by CSC, LiFOD achieves up to **400 Kbps** in data rate at a range of up to **6m** in SIGCOMM17 traffic. It is about **2.7** times better for throughput and **1.5** times better for communication range compared with the latest OpenVLC (average **150 Kbps** at 4m under optical interferences).

(2) Impact of incidence angle and position.

Because light beams emit and spread in the line-of-sight (LOS) manner, the pointing and direction setting is essential in high-speed OWC systems. We evaluate the influence of different facing angles and the receiver's relative locations as shown in the experimental schematic Figure 17 (b). The transmitter is fixed while the receiver's location and its facing angle are changed incrementally at 5° and 2cm from its base location L_0 and direction. We set the transmission distance from L_0 of the receiver to the transmitter at **3.5m** and the transmission frequency to **125KHz** for our two data traces.

As shown in Figure 17 (b), when the receiver is set at L_0, LiFOD can tolerate more unaligned angles. When the receiver is moved left or right in small ranges such as 2 or 4 cm, it is the same. For long-range location movement, throughput drops dramatically unless setting proper angle. The trend is consistent for two data traces. Thus, it is important for real-world usage of LiFOD to make sure the transmitter's light directly points to the receiver. However, this is consistent with normal usage habits of using lamps for our daily lighting.

(3) Throughput comparison with the state-of-art.

Finally, we make comparisons among LiFOD with state-of-art methods: OOK-CT, MPPM, and AMPPM in SmartVLC[38] shown in Figure18. We set the same transmission frequency to **125KHz** and distance to **3.5m**. OOK-CT is OOK with Compensation Time, it keeps the CS symbols' amplitude constant and only changes the

inserted number of CS symbols for dimming. Thus, OOK-CT, MPPM, and AMPPM are coupled-dimming-based OWC. We evaluate LiFOD with SIGCOMM17 and CAIDA19 data traces. We transmit OOK symbols without CSC bonus in LiFOD as a comparison.

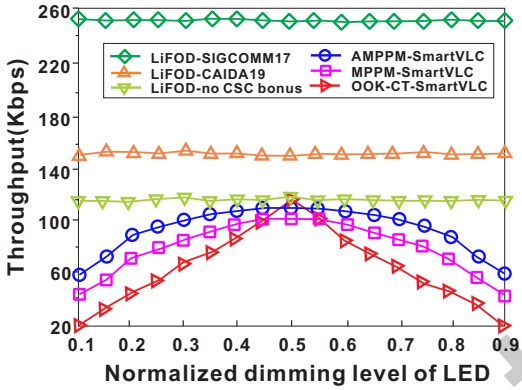

Fig. 18. Comparison with state-of-art[38].

First of all, our LiFOD throughput performances are better than **coupled-dimming**-based OWC methods in all scenarios. The reason is that LiFOD decouples the dimming with transmission and releases most times slots for standard data symbol transmission. Based on different CSC bonus ratios in various data traces, LiFOD for SIGCOMM17 traffic performs best and achieves **250 Kbps** in all dimming settings, which is an improvement of at least **110%** compared to AMPPM. Although lower than SIGCOMM17, LiFOD for CAIDA19 traffic which collects the daily network traffic of a city in the US still achieves **155 Kbps** in all dimming settings, which corresponds to at least a **34%** improvement over AMPPM in SmartVLC (the best throughput performance is **120 Kbps**).

Generalizability. The throughput improvement ratio in LiFOD is based on the bonus ratio of traffic. Other OWC platforms, such as the LiFi system, can apply LiFOD approach to improve their performance. Suppose the common OWC platform is improved in engineering or products such as robust symbol transmission and decoding at the **MHz/GHz** level. In that case, LiFOD can also be adopted to achieve the throughput improvement at the same boost ratio and may achieve the data rate at **hundreds of Mbps/Gbps** with fine-grained dimming support.

9.2.3 Real-time Bit Pattern Mining Performance.

Setup and assumptions. There are total 124 classes of bit segments (i.e., '00', ..., '111111') with the bit length less than or equal to 6 bits. Considering the significant labeling workload, we choose four 4-bits bit segment in exploration. They are '0000', '1111', '0011', and '0110'. For each class, we manually label that bit segment in 10 pieces for each bit stream of 30 varied PHY bit streams. Then we adopt dataset augmentation by adjusting grayscale, hue, saturation, and brightness to increase the dataset into the size of 72 images. Therefore, there are $72 \times 4 \times 10 = 2880$ total bit segment instances in the dataset. We adopt the small model of YOLOv5 (i.e., yolov5l.pt). We train the model on GPU Tesla V100S-PCIE-32GB. The model details: 267 layers, 46113663 parameters.

Confusion Matrix. As shown in Figure 19 (b), the trained model can differentiate these four bit segments without significant confusion. With the exception of the bit segment '0000', the bit segments' prediction accuracy are higher than 0.80. The prediction accuracy of bit segment '0000' is very low (i.e., 0.2). The reason is the trained model can not differentiate the '0000' and the background because the '0000' appears often in the background but we only label 10 of '0000' in an image. But this effect also reflects that the bit segment '0000' is the most frequent

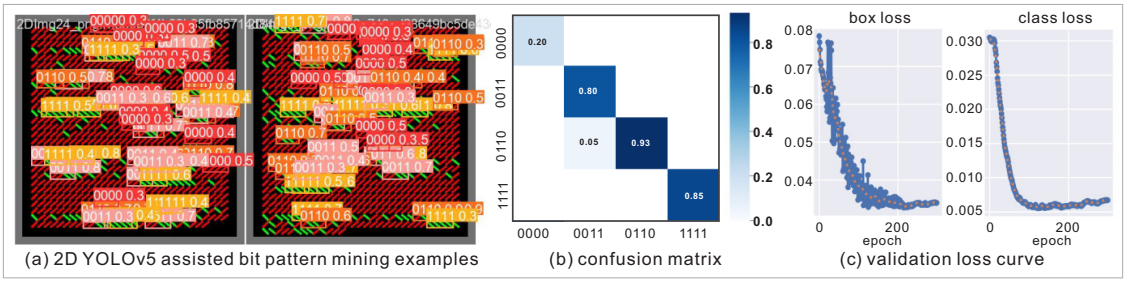

(a) 2D YOLOv5 assisted bit pattern mining examples (b) confusion matrix (c) validation loss curve

Fig. 19. The effectiveness of YOLO assisted bit pattern mining: (a) deep learning assisted bit pattern mining examples, (b) confusion matrix of 4 example bit segments, and (c) the validation loss curve of box loss and class loss in YOLOv5.

bit segment and can be chosen as one of the bit patterns. Due to the feature enhancement with coloring and directional design, the bit segments can be classified correctly, as shown in Figure 19 (a).

Validation Loss. We present two different training loss results in YOLO model: (1) bonding box loss, which demonstrates that generated bonding boxes are accurate, and (2) classification loss, which can reflect the accuracy of classification of different bit segments. As shown in Figure 19 (c), the validation losses of both box and class decrease significantly after 100 epochs. These results demonstrate the trained model works well to find and locate the specific bit segments.

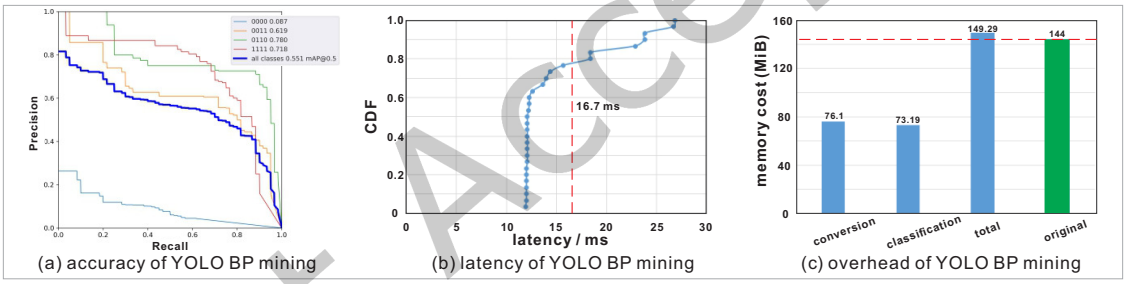

(a) accuracy of YOLO BP mining (b) latency of YOLO BP mining (c) overhead of YOLO BP mining

Fig. 20. YOLO assisted bit pattern mining performance compared with greedy based bit pattern mining.

Accuracy. We evaluate two cases of performance accuracy. First, we measure the detection accuracy of a specific bit segment, as shown in Figure 20 (a) and Figure 19 (b). As previously explained, with the exception of '0000', the bit segments have good prediction accuracy. Our goal is to find the several most frequent bit segments (e.g., 2) to be used as bit patterns. Our adopted the YOLO model can report how often a specific bit segment appears. Then we can decide which bit segment can be chosen as bit patterns. Given a result example, the trained model outputs there are 3 appearances of '0000', 18 of '0011', 12 of '0110' and 16 of '1111'. We choose '0000' (with most appearance but low recognition due to coarse labeling for dataset preparation) and '0011' (with the most number of recognition) as two bit patterns.

Latency. We evaluate the inference time of all bit segments as well as the choice of the 2 bit patterns. The CDF result is shown in Figure 20 (b). Our YOLO assisted bit pattern mining costs the constant time at a 20 ms level. There are about 80% time costs that are less than 16.7 ms, which makes the real-time bit pattern mining possible for LiFOD's practical communication. This differs from a case where time cost increases with the length of the bit pattern segments.

Overhead. We evaluate the memory cost for inference of all bit segments as well as the decision of 2 bit patterns. The CDF result is shown inf Figure 20 (c). The conversion from bit stream to the 2D bit matrix costs the average of 76.1 MiB and the YOLO model prediction costs the average of 73.19 MiB memory cost. The total memory cost of YOLO bit pattern mining is 149.29 MiB on average, which is the similar to the original bit pattern mining algorithm.

9.3 Discussion

9.3.1 About Two LEDs. In our current design of transmitter front-end, we design it with two LED lamps to provide constant light emission (i.e., B1) from one LED lamp and adjustable light emission (i.e., B2 - B1) from the other LED lamp, illustrated in Figure 8 and 16. Although the transmitter front-end consists of two LED lamps, it provides zero dimension and should be treated as a point light source. In the future, these two LED lamps can be integrated and encapsulated together as one LED lamp with two emission units.

9.3.2 Limitations. We discuss some limitations of LiFOD and potential overcoming solutions for overcoming them.

Strict Pointing Requirement. The LiFOD transmitter is a point light source and the LiFOD receiver is the single-pixel Photo Diode (PD). Thus, successful communication requires the strict pointing between the Tx and the Rx. To overcome this limitation, LiFOD can extend the emission area of Tx's front-end and the perception area of Rx (i.e., PD's area) without change the communication manner of point-to-point (i.e., p2p).

Indoor Setting Only. Currently, LiFOD is designed for an indoor setting with fine-grained dimming and boosted data rate for communication. However, the current LiFOD prototype is not practical for an outdoor setting considering the strong ambient light such as the sun light. We can adopt a physical light filter or light pass filter algorithms in optical signal processing to combat the strong ambient light for robust communication.

9.3.3 Future Direction. We list several research directions for future work here.

(1) Faster Transmission with FPGA. The current micro controller in LiFOD is BeagleBone Black, which provide several hundreds of transmission frequency bandwidth. In the future, we can exploit FPG[60, 61] or other faster micro controllers to provide GHz transmission frequency bandwidth for Gbps data rate improvement of LiFOD. **(2) Multiple Cell Handover.** In a real-world scenario for an indoor office, there are multiple LED lamps on the ceiling. Considering user movement, we can explore and design fast hand over approaches that use the compensation symbol as well. **(3) Mobile Scenario.** Besides the fixed location of the transmitter (e.g., on the ceiling), there are challenges when both the transmitter and the receiver are mobile. For example, if the transmitter is installed on a vehicle, the receiver can be installed on another vehicle for V2V communication. We can design a beam steering approach and signal enhancement in the mobile setting to provide robust and practical communication.

10 CONCLUSION

This paper leverages expanded dimming methods, utilizing compensation symbols as a side-channel for data transmission, to enhance throughput in OOK-based Optical Wireless Communication (OWC) networks. First, we design a lightweight greedy algorithm[62, 63] to identify bit patterns to maximize the total bonus bit performance in real-world traces. We also propose practical deep learning assisted bit pattern mining for the real-time communication for the upgraded LiFOD system. Then we use the preamble to notify CSC codes, dynamic thresholds, and estimate channel conditions for robust demodulation in the changing optical environment. Most importantly, we design non-flicker optical symbols and compensation symbol relocation scheme to support smooth lighting and communication with improved throughput. LiFOD can achieve up to **400 Kbps** throughput in the communication range up to **6m** with fine-grained dimming. Compared with SmartVLC at the same

transmission parameters, LiFOD improves more than **34%** and **110%** throughput for two real-world data traces respectively in all dimming levels.

REFERENCES

[1] Yanbing Yang, Jie Hao, and Jun Luo. 2017. CeilingTalk: Lightweight indoor broadcast through LED-camera communication. *IEEE TMC* (2017).

[2] Zeyu Wang, Zhice Yang, Qianyi Huang, Lin Yang, and Qian Zhang. 2019. ALS-P: Light Weight Visible Light Positioning via Ambient Light Sensor. In *Proceedings of INFOCOM*.

[3] Zhao Tian, Kevin Wright, and Xia Zhou. 2016. The darklight rises: Visible light communication in the dark. In *Proceedings of MobiCom*.

[4] Xiping Wu, Mohammad Dehghani Soltani, Lai Zhou, Majid Safari, and Harald Haas. 2021. Hybrid LiFi and WiFi networks: A survey. *IEEE Communications Surveys & Tutorials* 23, 2 (2021), 1398–1420.

[5] U.S. Department of Energy. 2022. Lighting Choices to Save You Money. (2022).

[6] Shilin Zhu, Chi Zhang, and Xinyu Zhang. 2017. Automating visual privacy protection using a smart led. In *Proceedings of MobiCom*.

[7] Nan Cen, Neil Dave, Emrecan Demirors, Zhangyu Guan, and Tommaso Melodia. 2019. LiBeam: Throughput-Optimal Cooperative Beamforming for Indoor Visible Light Networks. In *Proceedings of INFOCOM*.

[8] Pengfei Hu, Parth H Pathak, Xiaotao Feng, Hao Fu, and Prasant Mohapatra. 2015. Colorbars: Increasing data rate of led-to-camera communication using color shift keying. In *Proceedings of CoNEXT*.

[9] Yanbing Yang and Jun Luo. 2018. Boosting the throughput of LED-camera VLC via composite light emission. In *Proceedings of INFOCOM*.

[10] Xiao Zhang and Li Xiao. 2020. RainbowRow: Fast Optical Camera Communication. In *2020 IEEE 28th International Conference on Network Protocols (ICNP)*. IEEE, 1–6.

[11] Qing Wang, Marco Zuniga, and Domenico Giustiniano. 2016. Passive communication with ambient light. In *Proceedings of CoNEXT*.

[12] E Ramadhani and GP Mahardika. 2018. The technology of lifi: A brief introduction. In *IOP conference series: materials science and engineering*, Vol. 325. IOP Publishing, 012013.

[13] Philip Lundrigan, Neal Patwari, and Sneha K. Kasera. 2019. On-Off Noise Power Communication. In *Proceedings of MobiCom*.

[14] Yanbing Yang, Jun Luo, Chen Chen, Wen-De Zhong, and Liangyin Chen. 2019. SynLight: synthetic light emission for fast transmission in COTS device-enabled VLC. In *Proceedings of INFOCOM*.

[15] Minhao Cui, Yuda Feng, Qing Wang, and Jie Xiong. 2020. Sniffing visible light communication through walls. In *Proceedings of MobiCom*.

[16] Xiao Zhang and Li Xiao. 2020. Lighting extra data via owc dimming. In *Proceedings of the Student Workshop*. 29–30.

[17] Xiao Zhang, James Mariani, Li Xiao, and Matt W Mutka. 2022. LiFOD: Lighting Extra Data via Fine-grained OWC Dimming. In *2022 19th Annual IEEE International Conference on Sensing, Communication, and Networking (SECON)*. IEEE, 73–81.

[18] Xiao Zhang, Hanqing Guo, James Mariani, and Li Xiao. 2022. U-Star: An Underwater Navigation System based on Passive 3D Optical Identification Tags. In *The 28th Annual International Conference on Mobile Computing and Networking*.

[19] Xiao Zhang, Griffin Klevering, and Li Xiao. 2023. PoseFly: On-site Pose Parsing of Swarming Drones via 4-in-1 Optical Camera Communication. In *2023 IEEE 24th International Symposium on a World of Wireless, Mobile and Multimedia Networks (WoWMoM)*. IEEE, 1–10.

[20] Xiao Zhang, Griffin Klevering, James Mariani, Li Xiao, and Matt W Mutka. 2023. Boosting Optical Camera Communication via 2D Rolling Blocks. *Proceedings of IEEE/ACM International Symposium on Quality of Service* (2023).

[21] Xiao Zhang, Griffin Klevering, Juexing Wang, Li Xiao, and Tianxing Li. 2023. RoFin: 3D Hand Pose Reconstructing via 2D Rolling Fingertips. *Proceedings of 21st ACM International Conference on Mobile Systems, Applications, and Services* (2023).

[22] Xiao Zhang, Griffin Klevering, Xinyu Lei, Yiwen Hu, Li Xiao, and Tu Guanhua. 2023. The Security in Optical Wireless Communication: A Survey. *ACM Computing Surveys (CSUR)* (2023).

[23] Xiao Zhang, Griffin Klevering, and Li Xiao. 2022. Exploring Rolling Shutter Effect for Motion Tracking with Objective Identification. In *Proceedings of the Twentieth ACM Conference on Embedded Networked Sensor Systems*. 816–817.

[24] 2019. IEEE Standard for Local and metropolitan area networks–Part 15.7: Short-Range Optical Wireless Communications. *IEEE Std 802.15.7* (2019).

[25] Hongjia Wu, Qing Wang, Jie Xiong, and Marco Zuniga. 2017. SmartVLC: When smart lighting meets VLC. In *Proceedings of CoNEXT*.

[26] Pei Huang, Jun Huang, and Li Xiao. 2016. Exploiting Modulation Scheme Diversity in Multicarrier Wireless Networks. In *SECON*.

[27] Neminath Hubballi and Mayank Swarnkar. 2018. *BitCoding*: Network Traffic Classification Through Encoded Bit Level Signatures. *IEEE/ACM Transactions on Networking* (2018).

[28] N Muraleedharan, Anna Thomas, S Indu, and BS Bindhumadhava. A Traffic Monitoring and Policy Enforcement Framework for HTTP. In *2020 Third ISEA Conference on Security and Privacy (ISEA-ISAP)*. IEEE, 81–86.

[29] X. Wang, J. P. Linnartz, and T. Tjalkens. 2016. An Intelligent Lighting System: Learn User Preferences from Inconsistent Feedback. In *Proceedings of UbiComp*.

[30] Yang Yang, Zhimin Zeng, Julian Cheng, and Caili Guo. 2017. A novel hybrid dimming control scheme for visible light communications. *IEEE Photonics Journal* 9, 6 (2017), 1–12.
[31] Yang Yang, Zhimin Zeng, Julian Cheng, and Caili Guo. 2016. Spatial dimming scheme for optical OFDM based visible light communication. *Optics express* (2016).
[32] Fahad Zafar, Dilukshan Karunatilaka, and Rajendran Parthiban. 2015. Dimming schemes for visible light communication: the state of research. *IEEE Wireless Communications* 22, 2 (2015), 29–35.
[33] FK Yam and Zainuriah Hassan. 2005. Innovative advances in LED technology. *Microelectronics Journal* 36, 2 (2005), 129–137.
[34] Nikolay Zheludev. 2007. The life and times of the LED—a 100-year history. *Nature photonics* 1, 4 (2007), 189–192.
[35] Harald Haas, Liang Yin, Yunlu Wang, and Cheng Chen. 2015. What is lifi? *Journal of lightwave technology* 34, 6 (2015), 1533–1544.
[36] Muhammad Sarmad Mir, Borja Genoves Guzman, Ambuj Varshney, and Domenico Giustiniano. 2021. PassiveLiFi: rethinking LiFi for low-power and long range RF backscatter. In *Proceedings of the 27th Annual International Conference on Mobile Computing and Networking*. 697–709.
[37] J. Hao, Y. Yang, and J. Luo. 2016. CeilingCast: Energy efficient and location-bound broadcast through LED-camera communication. In *IEEE INFOCOM 2016 - The 35th Annual IEEE International Conference on Computer Communications*. 1–9.
[38] Hongjia Wu, Qing Wang, Jie Xiong, and Marco Zuniga. 2019. SmartVLC: Co-designing smart lighting and communication for visible light networks. *Transactions on Mobile Computing* (2019).
[39] Hui-Yu Lee, Hao-Min Lin, Yu-Lin Wei, Hsin-I Wu, Hsin-Mu Tsai, and Kate Ching-Ju Lin. 2015. Rollinglight: Enabling line-of-sight light-to-camera communications. In *Proceedings of MobiSys*.
[40] Mohammed SA Mossaad, Steve Hranilovic, and Lutz Lampe. 2015. Visible light communications using OFDM and multiple LEDs. *IEEE Transactions on Communications* (2015).
[41] CIE. 1931. chromaticity diagram. (1931).
[42] Tianxing Li, Chuankai An, Zhao Tian, Andrew T Campbell, and Xia Zhou. 2015. Human sensing using visible light communication. In *Proceedings of the 21st Annual International Conference on Mobile Computing and Networking*. 331–344.
[43] Chi Zhang and Xinyu Zhang. 2017. Pulsar: Towards ubiquitous visible light localization. In *Proceedings of the 23rd Annual International Conference on Mobile Computing and Networking*. 208–221.
[44] Ander Galisteo, Diego Juara, and Domenico Giustiniano. 2019. Research in visible light communication systems with OpenVLC1. 3. In *2019 IEEE 5th World Forum on Internet of Things (WF-IoT)*. IEEE.
[45] Junsu Jang and Fadel Adib. 2019. Underwater backscatter networking. In *Proceedings of the ACM Special Interest Group on Data Communication*.
[46] Raed Mesleh, Hany Elgala, and Harald Haas. 2012. LED nonlinearity mitigation techniques in optical wireless OFDM communication systems. *Journal of Optical Communications and Networking* 4, 11 (2012), 865–875.
[47] Francisco J. Escribano, José Sáez Landete, and Alexandre Wagemakers. 2019. Chaos-Based Multicarrier VLC Modulator With Compensation of LED Nonlinearity. *IEEE Trans. Communications* 67, 1 (2019), 590–598. DOI: http://dx.doi.org/10.1109/TCOMM.2018.2870874
[48] Kai Ying, Zhenhua Yu, Robert J Baxley, Hua Qian, Gee-Kung Chang, and G Tong Zhou. 2015. Nonlinear distortion mitigation in visible light communications. *IEEE Wireless Communications* 22, 2 (2015), 36–45.
[49] Tengjiao Wang, Fang Yang, Jian Song, and Zhu Han. 2020. Dimming techniques of visible light communications for human-centric illumination networks: State-of-the-art, challenges, and trends. *IEEE Wireless Communications* 27, 4 (2020), 88–95.
[50] Seong-Ho Lee. 2021. Dimming Control for Visible Light in a Wireless Identification System Using Manchester Code. *IEEE Sensors Letters* 5, 11 (2021), 1–4. DOI: http://dx.doi.org/10.1109/LSENS.2021.3126054
[51] CAIDA UCSD. 2017. SIGCOMM'17 anonymized internet traces. (2017).
[52] Vasilis K Papanikolaou, Panagiotis P Bamidis, Panagiotis D Diamantoulakis, and George K Karagiannidis. 2018. Li-Fi and Wi-Fi with common backhaul: Coordination and resource allocation. In *2018 IEEE wireless communications and networking conference (WCNC)*. IEEE, 1–6.
[53] Hossein Kazemi, Majid Safari, and Harald Haas. 2017. A wireless backhaul solution using visible light communication for indoor Li-Fi attocell networks. In *2017 IEEE International Conference on Communications (ICC)*. IEEE, 1–7.
[54] CAIDA UCSD. 2019. CAIDA'19 anonymized internet traces. (2019).
[55] Joseph Redmon, Santosh Divvala, Ross Girshick, and Ali Farhadi. 2016. You only look once: Unified, real-time object detection. In *Proceedings of the IEEE conference on computer vision and pattern recognition*. 779–788.
[56] Glenn Jocher. 2020. ultralytics/yolov5: v3.1 - Bug Fixes and Performance Improvements. https://github.com/ultralytics/yolov5. (Oct. 2020). DOI: http://dx.doi.org/10.5281/zenodo.4154370
[57] Anand Nayyar and Vikram Puri. 2016. A comprehensive review of beaglebone technology: Smart board powered by ARM. *International Journal of Smart Home* 10, 4 (2016), 95–108.
[58] K Durga Saranya, R Krishnamurthy, KNH Srinivas, TDNSS Sarveswara Rao, and IS Amiri. 2023. IoT-based health monitoring system using beaglebone black with optical sensor. *Journal of Optical Communications* 44, 3 (2023), 359–365.
[59] GSA. U.S. General Services Administration, 6.15 Lighting. ([n. d.]).

[60] Andrew Boutros and Vaughn Betz. 2021. FPGA architecture: Principles and progression. *IEEE Circuits and Systems Magazine* 21, 2 (2021), 4–29.
[61] Alexander Magyari and Yuhua Chen. 2022. Review of state-of-the-art FPGA applications in IoT Networks. *Sensors* 22, 19 (2022), 7496.
[62] Dieter Jungnickel and Dieter Jungnickel. 1999. The greedy algorithm. *Graphs, Networks and Algorithms* (1999), 129–153.
[63] Andrew R Barron, Albert Cohen, Wolfgang Dahmen, and Ronald A DeVore. 2008. Approximation and learning by greedy algorithms. (2008).